Journal of Materials Chemistry C

RSC Publishing

PAPER

View Article Online
View Journal | View Issue

Cite this: J. Mater. Chem. C, 2013, 1, 5527

Quantum dot/liquid crystal composite materials: self-assembly driven by liquid crystal phase transition templating

Andrea L. Rodarte, Ronald J. Pandolfi, Sayantani Ghosh* and Linda S. Hirst*

The isotropic to nematic liquid crystal (LC) phase transition is used to create organized assemblies of CdSe/ZnS core/shell quantum dots (QDs). Under controlled conditions, well dispersed QDs are expelled from the ordered domains of nematic LC into the remaining isotropic domains. The final LC phase produces three dimensional QD assemblies that are situated at the defect points in the LC volume. Through the luminescence of the QDs we are able to track the movement of the nanoparticles as the phase is formed as well as spectrally probe the resulting QD assemblies. Forster resonance energy transfer (FRET) measurements, combined with small angle X-ray scattering (SAXS) data reveal that the QD assemblies have a consistent inter-particle spacing of approximately 7.6 nm. Additionally, the location of the assemblies is shown to be controllable by utilizing beads as defect nucleation points.

Received 1st June 2013
Accepted 15th July 2013

DOI: 10.1039/c3tc31043d

www.rsc.org/MaterialsC

Introduction

Ensembles of nanoparticles (NPs) demonstrate collective behaviors that are fascinating variations on their bulk and single particle properties. These include novel electronic, magnetic and photonic effects[1,2] originating from inter-particle interactions, such as plasmonic resonances in metallic NP arrays,[3] superparamagnetism in assembled magnetic NPs[4] and Forster resonance energy transfer (FRET) between semiconductor NPs such as Quantum dots (QDs).[5] Controlling the assembly of interacting nanoparticles (NPs) is therefore an important goal in materials science as we aim to develop organized and close-packed two and three-dimensional NP superlattices to form metamaterials. Among all the NPs, QDs are particularly interesting for new metamaterials as these have unique size-tuneable properties arising from quantum confinement. Semiconducting particles are currently used in a wide variety of applications, including opto-electronic devices,[6] biochemical sensors,[7] photovoltaics, and as labels for biological microscopy.[8] This enhances the attractiveness of designing new multifunctional QD based materials.

The assembly of QDs (or any NPs) into clusters with a uniform packing density has been previously demonstrated in two and three dimensions using solution-based approaches,[9,10] but these methods produce static arrays that are not amenable to any kind of *in situ* manipulation. Creating macroscopic ordered assemblies of QDs with actively tunable properties is a challenging problem that we can address by leveraging the spatial and orientational flexibility offered by a liquid crystalline template. In this paper, we report a novel method to control the assembly of CdSe/ZnS core/shell QDs into both (1) uniformly packed assemblies of both spatially separated clusters and (2) interconnected web-like patterns using a templating method based on the isotropic to nematic liquid crystal phase transition. The structural and spectral features of the cluster assemblies are fully characterized, revealing a well-defined particle separation with corresponding distinctive FRET and PL lifetime characteristics.

Thermotropic liquid crystals exhibit different thermodynamic phases between the isotropic liquid and the solid crystalline phase as a function of temperature. The most well known LC mesophase is the nematic phase, where anisotropically shaped molecules exhibit short-range orientational order, defined by a local vector (the director). Surface functionalized NPs can be designed to disperse or assemble in different liquid crystal solvents. This behavior is critically dependent on the interaction between the NP surface ligands, the molecular details of the LC material and the LC phase. In an LC, it is not enough just to consider solvent properties of the individual molecules, we must also look at the effect of including a particle on liquid crystalline order. Fig. 1 demonstrates this idea. In an isotropic liquid phase, the rod-like LC molecules are randomly oriented and a particle with alkyl chain ligands will disperse in this mixture, with the LC molecules close to the particle orienting in a radial arrangement (Fig. 1a). If this same particle is placed into a medium with nematic order, there will be a competition between the tendency of the LC molecules to orient in a uniform direction as defined by the director and the radial distribution of molecules around the particle. This creates a topological mismatch between the director field at the particle

Department of Physics, School of Natural Sciences, University of California, Merced, CA 95343, USA. E-mail: lhirst@ucmerced.edu; sghosh@ucmerced.edu

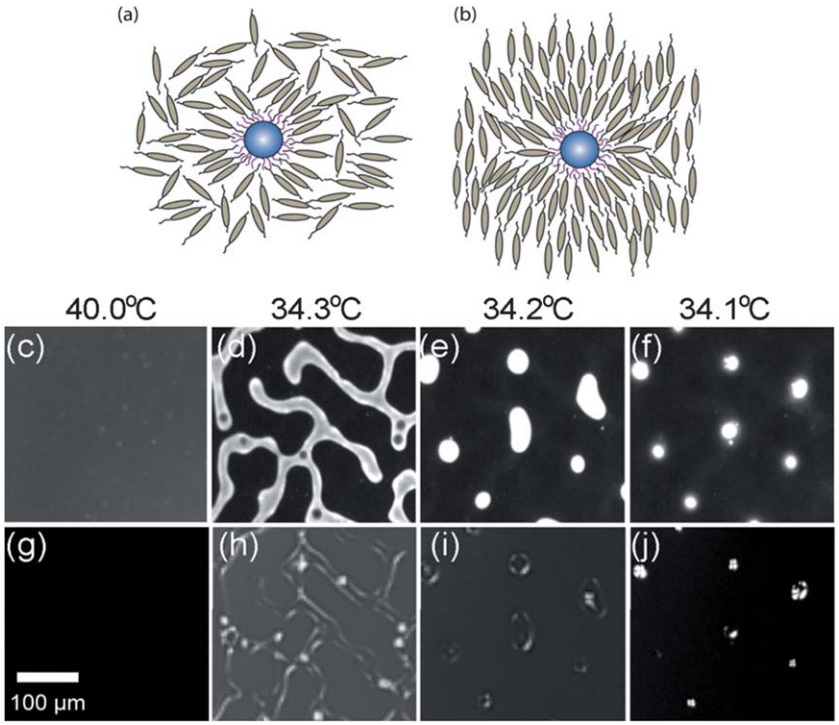

Fig. 1 Schematics of a QD in the (a) isotropic and (b) nematic phase, (c–f) fluorescence microscopy images of QD ensemble emission and (g–j) polarized microscopy images of the liquid crystal texture throughout the transition from isotropic (40 °C) into the nematic phase (34.1 °C).

surface and the nematic director far from the particle. The particle often creates a defect of +1 topological charge,[11] known as a radial hedgehog defect (Fig. 1b). There is much literature concerned with topological defects around colloidal particles included in a liquid crystal phase.[12] Most of these studies however, focus on the regime in which the particle is micron-scale. Large colloidal particles have been shown to form structures such as linear chains,[13,14] clusters,[15] arrays of defects[16] and particle stabilized gels[17] when dispersed in liquid crystal. Recently defects around colloidal particles were used to create controlled arrays in a liquid crystal matrix.[18]

There is an elastic energy cost whenever spherical particles are included in a nematic phase. Because of this effect we can expect the nematic phase to be a poorer solvent for our QDs than the isotropic phase, therefore promoting particle clustering in the nematic phase as a mechanism to minimize the free energy of the system. While there have also been some recent studies on liquid crystal–NP mixtures, these have generally been more focused on the effects of the dispersed NPs on the optical and electrical properties of the host LC phase.[19–22] Some of this has looked at NP assembly in the defects of discotic[23] and nematic LCs.[24–26] Recently our group has reported progress in QD dispersion in LC using GaAs and CdSe QDs, including their effects on the optical properties of cholesteric and nematic LCs.[27–31]

In this paper, we take advantage of the solvent properties of a nematic liquid crystal to organize and assemble QDs with octadecylamine surface ligands. At the transition, QDs preferentially localize to the shrinking isotropic phase domains, producing spatial patterns templated by nematic phase nucleation. We observe that after the phase transition is complete, QD clusters, localized at defect points in the LC texture are formed. By combining small angle X-ray diffraction with FRET measurements we are able to perform a more complete structural characterization than previously reported in similar systems and find that the QD clusters are at least 50 μm in diameter with an average inter-dot spacing of 7.6 nm. With the goal of assembling these clusters in an ordered array, we also demonstrate that cluster location can be controlled by the inclusion of additional micron-scale particles in the system, designed to nucleate defect points. These points attract the QD clusters as the system cools, providing a method to organize cluster assembly in a controlled fashion.

Results and discussion

For our study CdSe/ZnS core/shell QDs were chosen with octadecylamine surface ligands (NN Labs, core diameter 6.2 nm, absorption peak 600 nm) to promote homeotropic LC ordering at their surface. Fig. 1c–j show sequences of images collected almost simultaneously on the same QD/LC sample using fluorescence imaging and polarized optical microscopy (POM). We begin the experiment with an evenly dispersed distribution of QDs in the isotropic LC phase. On cooling slowly into the nematic phase, correlations between QD distribution and nematic phase formation are evident. The two imaging techniques are complementary; fluorescence reveals QD distribution in the LC medium, whereas POM provides a birefringence image, revealing liquid crystal alignment and orientation, including the location of defects. Fig. 1c–f are fluorescence

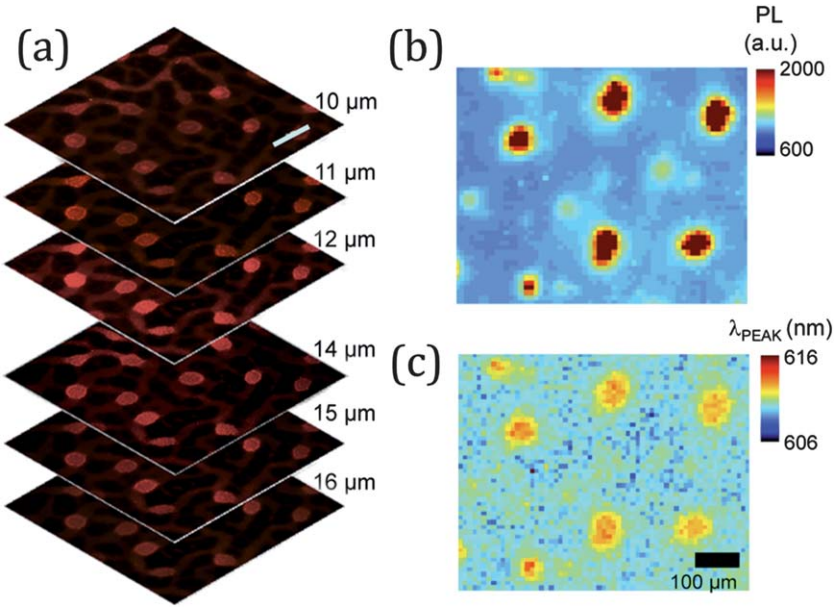

Fig. 2 (a) Confocal images of the sample at depths indicated and spatially resolved PL maps of the sample imaged in Fig. 1. Large scale scan showing (b) QD emission intensity and (c) peak emission wavelength. All figures have the same scale bar.

images that show the distribution of QDs as the system is slowly cooled into the nematic phase. Fig. 1g through j show the corresponding defect texture of the liquid crystal. Notice that at 40 °C (in the isotropic phase) the QDs are uniformly distributed across the imaged area. The small points of light are assumed to be clusters of QDs in the isotropic phase. On cooling to 34.3 °C, the isotropic to nematic transition begins and some LC areas nucleate, as seen in Fig. 1h. The corresponding fluorescence image for this temperature (Fig. 1d) clearly shows that the growing ordered domains expel most of the quantum dots from the nematic areas into nearby domains still in the isotropic phase. As the nematic domains grow and coalesce the QDs are seen to move into the remaining isotropic regions. The final locations of the QDs are in clusters located at defect points in the liquid crystal texture (Fig. 1f and j).

To further characterize QD distribution in an 8 μm thick LC cell we carried out scanning confocal microscopy. Using this technique we can see that the QD clusters are not localized to the center of the cell in a spherical aggregate, but in fact have a more columnar shape, bridging between the glass surfaces. Fig. 2a shows several individual confocal slices taken from a *z*-stack image of QDs in the LC cell. In these images, we also observe trails of lower-concentration QDs forming a network connecting the bright QD clusters similar to results observed for gold NPs by Milette *et al.*[25] These networks are likely formed during the early stages of phase transition similar to those seen in Fig. 1d. It is not surprising that all the QDs are not able to migrate to the defect points before the nematic phase transition is complete. From the images in Fig. 1 and 2, it is clear that the LC phase transition can be used to spatially organize QDs in the mixture, however optical microscopy alone cannot reveal further detail on QD cluster structure. For a deeper look at QD assembly structure on smaller length-scales, we used two different techniques, scanning photoluminescence (PL) confocal microscopy and small angle X-ray scattering (SAXS). Scanning PL confocal microscopy provides a high resolution image that includes spectral information. Fig. 2b shows a map of the spectrally-integrated peak intensity of the QD emission from the same sample shown in Fig. 1. From Fig. 2b we can note that there is PL emission across the entire imaged area. The clusters of QDs have an intensity ~2.5 times larger than the background, indicating that although there are clusters of QDs present, not all QDs are localized at those points. Fig. 2c shows a map of the corresponding peak wavelength for the sample. Comparing Fig. 2b and c we can see that the QDs assembled in clusters are redshifted by 3 nm compared to those in the background, indicating that they are close enough to exhibit Forster resonance energy transfer (FRET).[32]

Fig. 3 shows more detailed characterization of a single QD cluster. A higher resolution PL scan was performed on one cluster (Fig. 3a). Intensity mapping of QD emission reveals that the clusters are more intense at their center but the emission wavelength map in Fig. 3a reveals a relatively uniform red shift throughout the cluster core (Fig. 3b and c). It is interesting to note that areas of higher emission intensity do not produce a larger redshift. This suggests that although there are areas of higher QD concentration in the material, the relative spacing, and hence, the packing density, between QDs within that area remains constant. We can explain this effect by considering the likely structure of a cluster. The QDs used in this study are functionalized with octadecylamine surface ligands that define a minimum spacing between adjacent QDs. In addition, QD clusters likely form by an aggregation process, that may result in a fractal-like structure (Fig. 3f). Such a cluster, at the resolution of our imaging technique here, would appear uniform in intensity as a function of radius.

To further probe inter-particle distribution, spectrally and time-resolved PL data was collected in order to determine QD

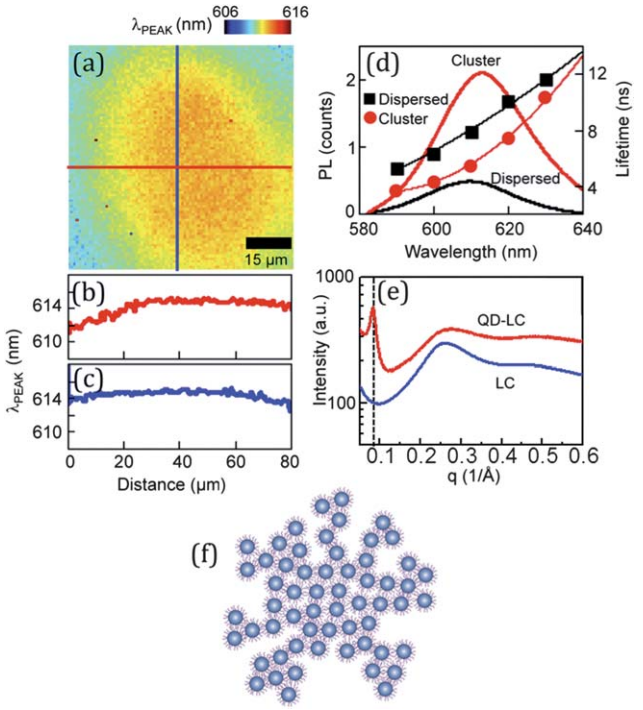

Fig. 3 (a) Spatially resolved PL maps of peak emission wavelength focused on a single QD cluster. Line cuts of (a) along (b) horizontal and (c) vertical directions (d) Spectral data from disperse and clustered QDs in nematic liquid crystal. Recombination times for dispersed (squares) and clustered (circles) have been overlaid. (e) Small angle X-ray scattering data from pure LC and QD–LC mixture. Data has been offset for clarity. (f) Schematic model of a QD aggregate.

recombination times. Fig. 3d shows emission spectra for dispersed QDs (black) and for a cluster of QDs (red). Corresponding recombination times at specific emission wavelengths are plotted across the spectrum. We observe that in both cases the recombination lifetimes increase with emission wavelengths, an indication of some energy transfer from the smaller (lower wavelength) QDs to the larger (longer wavelength) ones. Additionally, while both the dispersed and clustered QDs exhibit exponential decay with a single characteristic lifetime, the clustered QDs recombine at a faster rate at shorter wavelengths while appearing to catch up to, and even surpass (on extrapolation), the recombination rates at longer wavelengths. These observations imply there is increased FRET in the clustered QDs, in agreement with the red-shift seen in Fig. 3a. The efficiency of energy transfer, E_{FRET}, can be determined by comparing the lifetime of the QDs in the cluster, τ_C, and in solution, τ_S;

$$E_{FRET} = 1 - \left(\frac{\tau_C}{\tau_S}\right) \quad (1)$$

Using the lifetimes in Fig. 3d, we estimate a transfer efficiency of between 30.0 and 31.5% across the entire spectrum. The efficiency of the energy transfer can be related to the separation of donor and acceptor, r, by:

$$E_{FRET} = \frac{1}{1 + \left(\frac{r}{R_0}\right)^6} \quad (2)$$

where R_0 is the Förster radius, the distance at which the efficiency is 50%. Values for R_0 between separate donor and acceptor CdSe/ZnS QDs[33] should be modified to account for intra-ensemble energy transfer.[34] Taking these modifications into account we can estimate an R_0 of approximately 6.7 nm. Utilizing the measured efficiency we calculate an inter-dot spacing of 7.7 nm.

SAXS was carried out to complement the PL characterization of the QD clusters. A comparison of LC samples with and without QD clusters can be seen in Fig. 3e. The lower curve (blue) in Fig. 3e shows characteristic scattering from a nematic liquid crystal. The broad peaks correspond to average correlation distances between LC molecules. In the upper curve (red), QD clusters are present and a third peak is present at a lower **q**. We conclude that this peak, at 0.082 $Å^{-1}$, represents the scattering from QDs located in the clusters with an average QD correlation distance of 7.6 nm. This calculated value seems to indicate close-packing between the QDs. The nematic peaks are unchanged in this QD sample, as expected, since such a low concentration of QDs when dispersed, should have no significant effect on the bulk structure of the LC phase. In general, our nematic liquid crystal medium forms clusters containing QDs close enough to allow energy transfer, but in a typical sample (Fig. 1), the clusters nucleate with a fairly random spatial distribution, guided by the kinetics of the phase transition. For device applications it would be desirable to predict where QD clusters will form and to direct their assembly. To work towards a controllable mechanism for QD cluster assembly, we used a sample geometry in which defects are located in particular spots – prefabricated liquid crystal test cells (Instec Inc.). Randomly scattered 5 μm polystyrene beads are used to maintain an even spacing between the glass plates and for our purposes, each bead acts as a nucleation point for a defect in the LC texture. Now, instead of allowing the QD clusters to form in an uncontrolled distribution, we observed the QD clusters to preferentially locate at the pre-seeded defect points in an otherwise well aligned nematic phase. Fig. 4 shows fluorescence imaging of the 5CB–QD mixture cooling in a homeotropically aligned LC cell. The spacer beads can be identified as black dots in these images in Fig. 4a–d and it is clear that each bead visible in the image nucleates a QD cluster. These images also reveal an interesting web-like pattern connecting the final clusters also seen in Fig. 2a. The PL maps in Fig. 4e and f from another area in the same sample show numerous small clusters each with a stronger but more localized redshift than observed for the samples prepared without large beads.

When small particles are introduced into an LC phase, the local orientation of the molecules is disturbed. The LC molecule responds to the particle's surface and the presence of a particle creates an elastic deformation of the nematic phase (Fig. 1b). The QDs with octadecylamine ligands used here generate a local splay deformation of the LC director when dispersed and a hedgehog defect. The elastic energy cost of including particles can be minimized by clustering. This explains the difficulty often encountered in trying to disperse different nanoparticles in a liquid crystal phase. In the isotropic phase this elastic deformation problem is eliminated and particles can disperse more

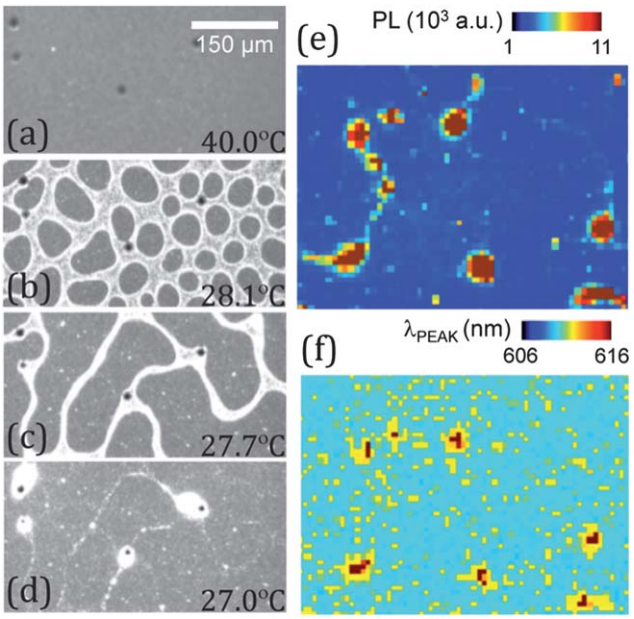

Fig. 4 (a–d) Fluorescence microscopy images of a QD ensemble cooling in a cell seeded with polystyrene beads (dark spots in (a)). The QD clusters are centered around the beads. Corresponding QD PL maps showing peak intensity (e) and peak wavelength (f) for a section of the cell. All figures have the same scale bar.

readily provided the LC acts as a reasonably good solvent. In our experiments, as the LC phase begins to nucleate and regions of ordered molecules appear and grow, we also observe that previously uniformly dispersed QDs move to occupy the remaining and shrinking isotropic domains. This 'steric sorting', similar to phase separation is explained by considering the energy cost of inserting a single QD into the nematic phase any deformation of the uniform director field will result in an increase in free energy. An additional consequence of this sorting phenomena is that nanoparticles tend to form web-like networks reminiscent of the patterns seen as the nematic phase forms, with QDs concentrated at certain points in the material (Fig. 2 and 4).

Arrays of large colloidal particles have recently been seen to assemble into well-defined colloidal crystals mediated by the attractive potentials between different topological defects that form around the particles.[18] Experimentally, the idea of using defect attractive potentials to assemble particles has not yet been extended to defects containing particles as small as QDs. In a recent study, however, the interactions between 150 nm particles were shown to be long ranged (~1 μm) and relatively weak (<5 k_BT), therefore appropriate for mediating reversible associations.[35] We expect that these effects contribute to observed nanoparticle clustering in the LC phase since particle-containing defects may be weakly attracted to each other. Quantification of this effect will make a fascinating subject for future work as we move toward the idea of directing the assembly of different nanoparticles into more well-defined lattice structures.

Conclusions

In conclusion, we demonstrate a method for the soft assembly of quantum dots in a composite material. Such materials, incorporating the optical properties of nanoparticles with the processability of liquid crystal are desirable for applications where solutions can be used to generate materials in a desired geometry or coated on a surface. The interaction between LC ordering and particle distribution is used to direct QD pattern formation at the phase transition, resulting in web-like networks, including columnar structures between the glass plates and QD clusters. Inside the clusters the QDs have a consistent interparticle spacing of approximately 7.6 nm, allowing for FRET efficiencies of approximately 30%. We also demonstrate a mechanism for controlling localization of the QD clusters, using defect-generating beads. Ordered clusters of nanoparticles created by liquid crystal templating represent a new class of soft-assembled metamaterials, similar to nanoparticle superlattices. The ideas presented in this paper can easily be expanded to metallic and magnetic nanoparticles by carefully selecting for particle size, surface ligands and the liquid crystal host, creating a wide variety of new materials and applications.

Experimental section

Composite material preparation and imaging

Nematic liquid crystal 4′-pentyl-4-biphenylcarbonitrile (5CB, Sigma Aldrich) is mixed with 2 mg ml^{-1} octadecylamine coated CdSe quantum dots (NN Labs) in toluene to a concentration of 0.02–0.04 wt%. Some residual toluene can be left in the material using this method, reducing the isotropic transition temperature by a few degrees. The QD–LC mixture is bath sonicated above the LC clearing temperature (43 °C) for a minimum of 5 hours to obtain even QD dispersion in the isotropic medium – verified by optical microscopy. A nematic material can be aligned such that the director is uniform over a large area using an alignment layer. A glass slide is cleaned, dip coated with aqueous hexadecyltrimethylammonium bromide (CTAB, Sigma Aldrich) and dried under nitrogen. This coating induces a homeotropic liquid crystal alignment (molecules oriented with their long axis perpendicular to the glass). Samples are sealed with a similarly coated glass cover slip. A Linkham LTS350 hot-stage maintained at 40 °C is used to initially keep the material in the isotropic phase.

Images are captured using a Leica DM2500P upright microscope equipped with a Q-image Retiga camera. This system allows us to observe QD dispersion in the isotropic fluid, while imaging the liquid crystal texture using polarized optical microscopy (POM). LC materials are optically anisotropic, therefore spatial variation in director orientation can be imaged using POM. In the homeotropic geometry used in this experiment, a uniformly aligned nematic appears dark when viewed between crossed polarizers. Defect points are visible and typically take the appearance of bright crosses. Confocal imaging was also carried out using a Nikon Eclipse Ti microscope with a 561 nm excitation laser and a z resolution of ~0.75 μm.

Photoluminescence spectroscopy

A 532 nm continuous wave excitation laser is focused on the sample through a high NA objective to produce a diffraction-limited

spot of diameter ~600 nm. Thin LC–QD films similar to those used for microscopy and enclosed in glass slides were mounted on a motorized 3D scanning stage with a 40 nm lateral resolution. Emitted PL from the QDs is collected by the same objective and dispersed by an Acton 300i spectrometer onto a thermoelectrically cooled CCD detector (spectral resolution ~ 0.18 nm). A selected sample area is raster-scanned to create spatially resolved PL maps.

Time resolved photoluminescence spectroscopy

A 420 nm photo-excitation pulse using the frequency-doubled output of a tunable Ti:sapphire laser with a 76 MHz (13 ns) repetition rate and 150 fs pulse width was used. The excitation power density is kept constant at 45 W cm^{-2}. Time-resolved data are collected using a single photon avalanche detector coupled to a time-correlated single photon counting system (PicoHarp 300) with an instrument response function of 12 ps. Time-resolved PL traces are extracted at a series of emission wavelengths for the sample.

Small angle X-ray scattering (SAXS)

Measurements were carried out on Beamline 4-2 at Stanford Synchrotron Radiation Laboratory. LC–QD mixtures were prepared as described earlier with 0.04 wt% quantum dots dispersed in nematic liquid crystal and pipetted into 1.5 mm quartz X-ray capillaries for unaligned (powder) scattering and exposed to an 11 keV X-ray beam for 0.5 s. Diffraction patterns are recorded on a CCD detector, then plotted as integrated intensity as a function of **q**, the scattering vector using the SASTOOL analysis software available at the beamline.

Acknowledgements

The authors would like to acknowledge generous funding from UC MEXUS and UC MERI.

Notes and references

1 M. Quinten, A. Leitner, J. R. Krenn and F. R. Aussenegg, *Opt. Lett.*, 1998, **17**, 1331.
2 C.-Y. Cho, S.-J. Lee, S.-H. Hong, S.-M. Lee, Y.-H. Cho and S.-J. Park, *Appl. Phys. Lett.*, 2011, **98**, 051106.
3 A. O. Govorov, G. W. Bryant, W. Zhang, T. Skeini, J. Lee, N. A. Kotov, J. M. Slocik and R. R. Naik, *Nano Lett.*, 2006, **6**(5), 984.
4 C. Binns, M. J. Maher, Q. A. Pankhurst, D. Kechrakos and K. N. Trohidou, *Phys. Rev. B: Condens. Matter Mater. Phys.*, 2002, **66**, 184413.
5 S. A. Crooker, J. A. Hollingsworth, S. Tretiak and V. I. Klimov, *Phys. Rev. Lett.*, 2002, **89**(18), 186802.
6 T.-H. Kim, K.-S. Cho, E. K. Lee, J. Chae, J. W. Kim, D. H. Kim, J.-Y. Kwon, G. Amaratunga, S. Y. Lee, B. L. Choi, Y. Kuk, J. M. Kim and K. Kim, *Nat. Photonics*, 2011, **5**, 176.
7 E. R. Goldman, I. L. Medintz, J. L. Whitley, A. Hayhurst, A. R. Clapp, H. T. Uyeda, J. R. Deschamps, M. E. Lassman and H. Mattousi, *J. Am. Chem. Soc.*, 2005, **127**, 6744.
8 X. Michalet, F. F. Pinaud, L. A. Bentolila, J. M. Tsay, S. Doose, J. J. Li, G. Sundaresan, A. M. Wu, S. S. Gambhir and S. Weiss, *Science*, 2005, **307**, 538.
9 T. P. Bigioni, X.-M. Lin, T. T. Nguyen, E. I. Corwin, T. A. Witten and H. M. Jaeger, *Nat. Mater.*, 2006, **5**, 265.
10 A. Pucci, M.-G. Willinger, F. Liu, X. Zeng, V. Rebuttini, G. Clavel, X. Bai, G. Ungar and N. Pinna, *ACS Nano*, 2012, **6**(5), 4382.
11 D. Andrienko, G. Germano and M. P. Allen, *Phys. Rev. E: Stat., Nonlinear, Soft Matter Phys.*, 2001, **63**, 04170.
12 R. W. Ruhwandl and E. M. Terentjev, *Phys. Rev. E: Stat. Phys., Plasmas, Fluids, Relat. Interdiscip. Top.*, 1997, **55**(3), 2958.
13 P. Poulin, H. Stark, T. C. Lubensky and D. A. Weitz, *Science*, 1997, **275**, 1770.
14 J.-C. Loudet, P. Barois and P. Poulin, *Nature*, 2000, **407**, 611.
15 P. Poulin and D. A. Weitz, *Phys. Rev. E: Stat. Phys., Plasmas, Fluids, Relat. Interdiscip. Top.*, 1998, **57**(1), 626.
16 M. Yada, J. Yamamoto and H. Yokoyama, *Langmuir*, 2002, **18**, 7436.
17 M. Zapotocky, L. Ramos, P. Poulin, T. C. Lubensky and D. A. Weitz, *Science*, 1999, **283**, 209.
18 I. Musevic, M. Skarabot, U. Talec, M. Ravnik and S. Zumer, *Science*, 2006, **313**, 954.
19 H. Qi, B. Kinkead and T. Hegmann, *Adv. Funct. Mater.*, 2008, **18**, 212.
20 L. O. Doglov and O. V. Yaroshchuk, *Colloid Polym. Sci.*, 2004, **282**, 1403.
21 A. Szilagyi, G. Fetter and M. Zrinyi, *J. Therm. Anal. Calorim.*, 2005, **82**(2), 525.
22 N. Kanayama, O. Tsutsumi, A. Kanazawa and T. Ikeda, *Chem. Commun.*, 2001, 2640.
23 S. Kumar and V. Lakshminarayanan, *Chem. Commun.*, 2004, 1600.
24 M. Urbanski, B. Kinkead, T. Hegmann and H.-S. Kitzerow, *Liq. Cryst.*, 2010, **37**(9), 1151.
25 J. Milette, S. J. Cowling, V. Toader, C. Lavigne, I. M. Saez, R. B. Lennox, J. W. Goodby and L. Reven, *Soft Matter*, 2012, **8**, 173.
26 E. R. Soule, J. Milette, L. Reven and A. D. Rey, *Soft Matter*, 2012, **8**, 2860.
27 L. S. Hirst, J. Kirchoff, R. Inman and S. Ghosh, *Proc. SPIE*, 2010, **7618**(1), 76180F.
28 Y. Verma, R. Inman, C. Ferri, H. Mirafzal, S. Ghosh, D. Kelley, L. Hirst, W. Chin and S. Ghosh, *Phys. Rev. B: Condens. Matter Mater. Phys.*, 2010, **82**, 035430.
29 A. L. Rodarte, C. Gray, L. S. Hirst and S. Ghosh, *Phys. Rev. B: Condens. Matter Mater. Phys.*, 2012, **85**, 035430.
30 A. L. Rodarte, G. V. Shcherbatyuk, L. Shcherbatyuk, L. S. Hirst and S. Ghosh, *RSC Adv.*, 2012, **2**, 12759.
31 J. Mirzaei, M. Reznikov and T. Hegmann, *J. Mater. Chem.*, 2012, **22**, 22350.
32 T. Forster, *Discuss. Faraday Soc.*, 1959, **27**, 7.
33 C. R. Kagan, C. B. Murray, M. Nirmal and M. G. Bawendi, *Phys. Rev. Lett.*, 1996, **76**(9), 1517.
34 M. Lunz, A. L. Bradley, V. A. Gerard, S. J. Byrne, Y. K. Gun'ko, V. Lesnyak and N. Gaponik, *Phys. Rev. B: Condens. Matter Mater. Phys.*, 2011, **83**, 115423.
35 G. M. Koenig, J. J. de Pablo and N. L. Abbott, *Langmuir*, 2009, **25**(23), 13318.

